Journal of Sound and Vibration (1998) **217**(3), 419–434
Article No. sv981810

ADAPTIVE PERIODIC DISTURBANCE CANCELLATION IN A SET-UP OF TWO CRYOCOOLERS

A. P. Rijpma, J. F. C. Verberne, E. H. R. Witbreuk†, P. C. Bruins‡ and H. J. M. ter Brake

Department of Applied Physics, *University of Twente*, *PO Box* 217, 7500 *AE Enschede*, *The Netherlands*

(*Received* 12 *March* 1997, *and in final form* 27 *April* 1998)

The work presented describes adaptive periodic disturbance cancellation as applied to the vibration of two cryocoolers. The coolers are driven by linear motors. The periodic input signal necessary to reduce the disturbance is calculated by vibration measurements using the system's frequency response. It is subsequently added to the drive voltage. This leads to a complete disturbance rejection in only one control step. The experimental results show excellent convergence within the limits of the vibration sensor resolution. A method of vibration control is thus described that is not only capable of reducing the vibrations at the drive frequency of the coolers, but also at multiple harmonics. For example, this means the vibrations are reduced from 1 and 0·2 ms^{-2} to 0·02 and 0·01 ms^{-2}, respectively for the various moving elements.

1. INTRODUCTION

The work described is part of a project aimed at the application of magnetocardiography under clinical conditions. Magnetocardiography (MCG) is comparable to the more widespread Electrocardiography (ECG) technique in that both methods measure the electrical activity of the heart muscle. The major difference is that ECG records differences in the electric potential over the body surface and MCG measures the magnetic field outside the body.

The magnitude of the heart's magnetic field ranges typically from 10 to 100 pT. The relevant frequency range is from 1 to 100 Hz. Since the magnetic fields to be measured are extremely weak, SQUIDs are used for MCG measurements. SQUID is an acronym for Superconducting QUantum Interference Device [1]. A SQUID

† Currently at: Tulip Computers International, Rosmalen, The Netherlands.
‡ Currently at: Signaal USFA, Eindhoven, The Netherlands.

0022–460X/98/430419 + 16 $30.00/0

has to be cooled below its critical temperature T_c in order to become superconducting. Classical or low-T_c materials become superconducting around 10 K. We, however, use SQUIDs made from ceramic or high-T_c materials which reduces the cooling requirements to about 80 K [1].

The MCG-technique is applied for several years mainly under laboratory conditions. This implies the use of an expensive and fixed magnetically shielded room. The emphasis of the present research project is to design an apparatus allowing clinical use of the MCG-technique. Price and mobility considerations exclude the use of a magnetically shielded room. As flexibility requires the realization of a turn-key apparatus, the SQUID sensors are to be cooled by cryocoolers as opposed to a cryogen such as liquid nitrogen (boiling point 77 K) [2].

Operation of an MCG-apparatus in a magnetically unshielded environment implies that, among other noise sources, movement of the magnetic sensors (SQUIDs) themselves may lead to significant disturbances [3]. For instance, rotation of the sensors in the earth's magnetic field (50 μT) by a mere 10^{-6} rads, will yield an equivalent field change of roughly 50 pT in the magnetometers.

Since for practical realization the cryocoolers will be situated close to the SQUID sensors, they will constitute a source of magnetic disturbances. These can be described by three effects: magnetic fields from currents powering the coolers, vibration of cooler parts and induced sensor vibration. The predominant 50 Hz mains frequency is to be removed from the sensor output by applying notch filtering. This will also remove the bulk of the cryocooler disturbances, since these are powered at the same frequency. However, to minimise the possible cooler disturbance at other frequencies through non-linear effects, the aim is to reduce the cryocooler vibrations as much as possible.

To this end a control system was developed, which is described in the following sections. First, in section 2, the cryocoolers are characterized. In section 3, both the basic control algorithm and its adaptation to our specific application are described. In section 4 attention is paid to the experimental identification of the cryocooler behaviour. In section 5 the hardware used in the experiments is described and the paper is concluded with the results obtained in section 6.

2. CRYOCOOLERS

The cryocoolers used are manufactured by Signaal USFA (type 7058) [4]. Their cooling power amounts to 1·5 W at 80 K and their drive frequency is 50 Hz, which coincides with the mains frequency. Each cooler consists of a compressor and a cold head as depicted in Figure 1. According to the Stirling cycle [5], expansion of the gas mainly occurs at the cold tip, whereas the compression of the gas is primarily achieved in the remaining space.

The two pistons of the compressor are driven by linear AC-motors. Each consists of a coil surrounded by a permanent magnetic field. Since the coil is fixed to a piston, motion is accomplished by feeding a current to the coil. Thus, the

pistons create a pressure wave in the working gas. This pressure wave drives the motion of the displacer located in the cold head. The masses of pistons and displacer, combined with mechanical springs and gas forces, form a resonant system tuned to the drive frequency.

As the two pistons of the compressor operate in counter-phase (the so-called "dual opposed piston compressor"), substantial vibration reduction is established for the compressor, leaving the cold head as a major source of vibration. In order to reduce this vibration to some extent, we decided to use two coolers in a back-to-back arrangement as shown in Figure 2. The single rigid structure containing the two cold heads, will be referred to as the displacer unit. In order to study and suppress the remaining vibrations, both the compressors and the displacer unit are mounted on thin plates to allow free motion along their axes. These plates in turn are connected to a heavy base plate [6]. The SQUID-magnetometers are not present in the current set-up. They are planned to be situated about 30 cm from the displacer unit [2]. The vibrations are measured by acceleration transducers placed on the compressors and the displacer unit. The combination of the two cold heads to a single displacer unit reduced the axial vibrations at 50 Hz from about 4 ms^{-2} per cold head to about 0·2 ms^{-2} for the unit [6]. The axial vibration of a compressor without any control is typically 1 ms^{-2} at the 50 Hz drive frequency.

We decided to reduce the vibrations further by tuning the coil voltages. A promising algorithm for this purpose was presented by Wu [7] and Boyle *et al*. [8]. This algorithm uses the measured vibrations and the system's frequency response to determine the necessary changes in the coil voltages.

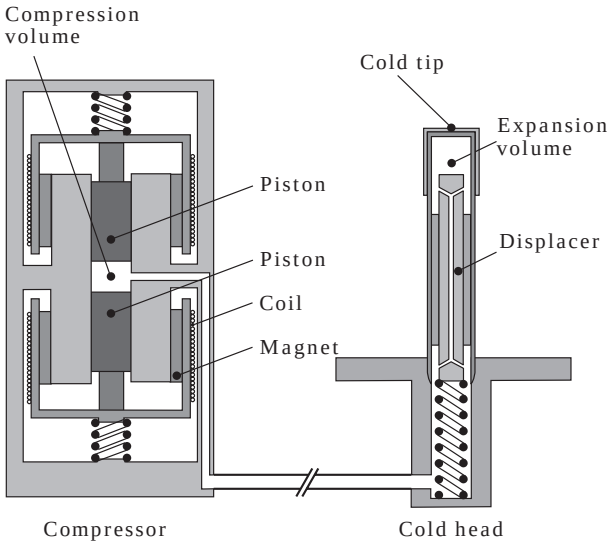

Figure 1. Cross section of the type 7058 cryocooler (courtesy of Signaal USFA [4]).

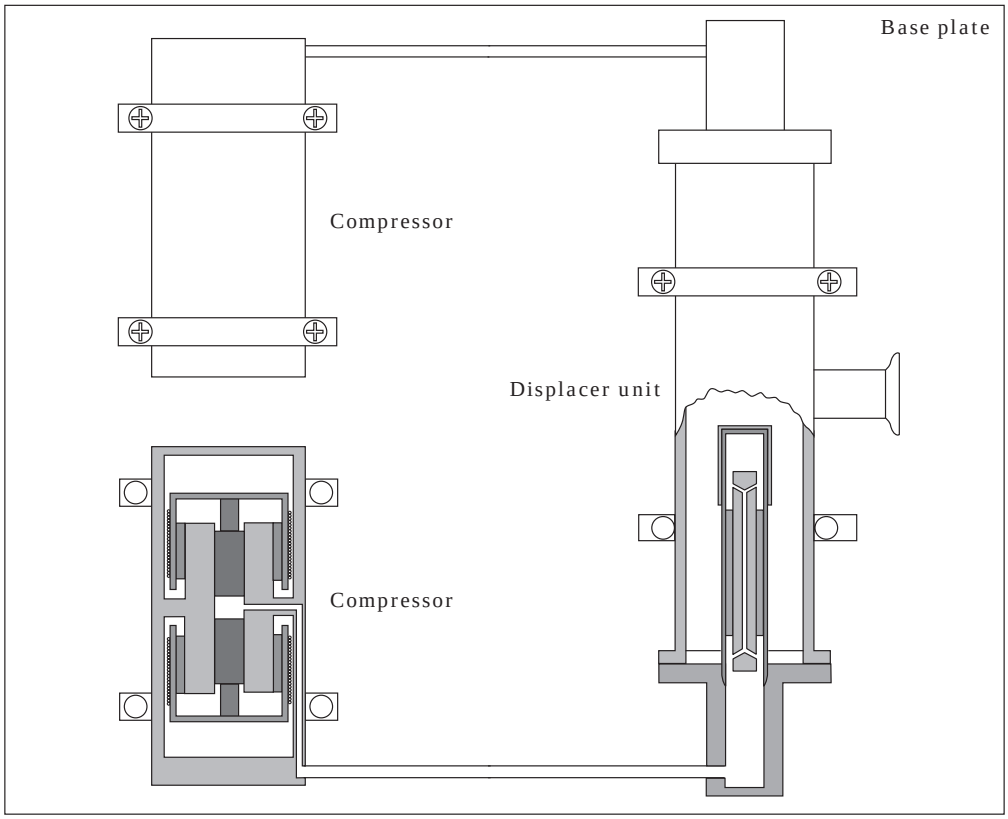

Figure 2. Experimental base plate with the two cold heads in dual opposed arrangement to the right and the two compressors to the left.

3. CONTROL SYSTEM

3.1. BASIC ALGORITHM

First, the algorithm is derived for a single-input–single-output situation as depicted in Figure 3. Here, $\mathbf{A}(k)$ is the system acceleration resulting from a transfer function $\mathbf{H}$ and a disturbance $\mathbf{D}$. The function $\mathbf{H}$ relates the system input voltage $\mathbf{V}(k)$ to its acceleration. Voltage $\mathbf{V}_0$ is the drive voltage and $\mathbf{V}_c(k)$ is the control voltage after control step k. The voltage generated by the algorithm should be designed to reduce the acceleration $\mathbf{A}$ as measured by the acceleration sensor $\boldsymbol{\beta}$. Since the disturbance is assumed to contain a limited number of harmonics of the cooler drive frequency, the control algorithm consists of the following two steps.

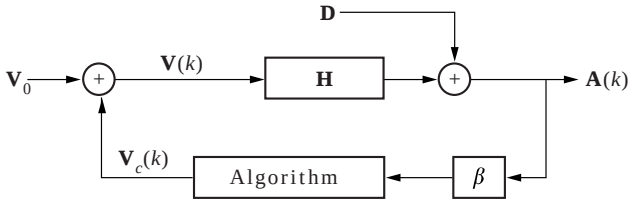

Figure 3. Diagram of the basic control system.

First, a discrete fourier transform (DFT) of the measured acceleration is calculated. Then, the control voltage $\mathbf{V}_c$ is appropriately changed.

Neglecting the transient phenomena due to a change in the control voltage, one may write the acceleration $\mathbf{A}$ as a summation of the disturbance $\mathbf{D}$ and the system's output $\mathbf{HV}$:

$$\mathbf{A}(k, \mathrm{j}n\Omega) = \mathbf{D}(\mathrm{j}n\Omega) + \mathbf{H}(\mathrm{j}n\Omega)\mathbf{V}(k, \mathrm{j}n\Omega). \tag{1}$$

Here, $n = 1, \ldots, N$ is introduced to denote the various harmonics of the drive frequency Ω present in the system vibrations. The parameter k represents the control time step. In this paper the notation will be simplified, using n as a subscript:

$$\mathbf{A}_n(k) = \mathbf{D}_n + \mathbf{H}_n\mathbf{V}_n(k). \tag{2}$$

Ideally, acceleration $\mathbf{A}_n(k+1)$ at a time step $k+1$ should become zero by means of the control. It is clear from equation (2) that this implies

$$\mathbf{V}_n(k+1) = \mathbf{V}_n(k) - \mathbf{A}_n(k)/\mathbf{H}_n. \tag{3}$$

In the analysis, it is assumed that the transfer function $\mathbf{H}(\mathrm{j}\omega)$ from control voltage to acceleration is linear. Furthermore, only the drive frequency and a restricted number N of higher harmonics are assumed relevant in the vibrations. Both conditions are met as will be shown in section 6.

For implementation of the algorithm, we use the following equations:

$$v_c(t) = \sum_{n=1}^{N} v_{c,n}(t) = \sum_{n=1}^{N} [\gamma_n(k)\sin(n\Omega t) + \delta_n(k)\cos(n\Omega t)], \tag{4}$$

$$\gamma_n(k+1) = \gamma_n(k) + \frac{2A_{i,n}\cos(\psi_n) - 2A_{r,n}\sin(\psi_n)}{H_n}, \tag{5}$$

$$\delta_n(k+1) = \delta_n(k) - \frac{2A_{i,n}\sin(\psi_n) + 2A_{r,n}\cos(\psi_n)}{H_n}. \tag{6}$$

The lower case v_c is used for the representation of the control voltage $\mathbf{V}_c$ in the time domain. H_n and ψ_n are the amplitude and phase of the system transfer function for the drive frequency's nth harmonic. $A_{r,n}$ and $A_{i,n}$ are the real and imaginary components of the DFT of the acceleration.

Derivation of equations (4)–(6) was carried out analogously to Wu's treatment in reference [7]. One important difference with respect to Wu's results is the absence of $\mathbf{V}_{c,n}$—the control voltage amplitude—in one of the denominators, as this leads to mathematical problems when $\mathbf{V}_{c,n}$ is (close to) zero. Another advantage of the above equations is that no linearization is used in deriving them. This leads to a perfect one-step control in the case that the transfer function is known exactly.

3.2. APPLICATION TO CRYOCOOLERS

We now proceed from the basic algorithm as depicted in Figure 3 to its application as presented in Figure 4. Compared to the single-input–single-output system presented in Figure 3 with only one transfer function **H**, we now discern several transfer functions: They correspond to the acceleration response of each of the three mechanical components to the four voltage inputs. We start by describing the system behaviour using the compressor coil voltages $\mathbf{V}_1$ to $\mathbf{V}_4$, which are comparable to the system input **V** used in section 3.1. Analogously to equation (1), the system behaviour is described by the following complex matrix:

$$\begin{Bmatrix} \mathbf{A}_1 \\ \mathbf{A}_2 \\ \mathbf{A}_3 \end{Bmatrix}(k) = \begin{Bmatrix} \mathbf{D}_1 \\ \mathbf{D}_2 \\ \mathbf{D}_3 \end{Bmatrix} + \begin{bmatrix} \mathbf{H}_{11} & \mathbf{H}_{21} & \mathbf{H}_{31} & \mathbf{H}_{41} \\ \mathbf{H}_{12} & \mathbf{H}_{22} & \mathbf{H}_{32} & \mathbf{H}_{42} \\ \mathbf{H}_{13} & \mathbf{H}_{23} & \mathbf{H}_{33} & \mathbf{H}_{43} \end{bmatrix} \begin{Bmatrix} \mathbf{V}_1 \\ \mathbf{V}_2 \\ \mathbf{V}_3 \\ \mathbf{V}_4 \end{Bmatrix}(k). \quad (7)$$

In this equation $\mathbf{A}_1$, $\mathbf{A}_2$ and $\mathbf{A}_3$ are the acceleration of respectively the compressors and the displacer unit; $\mathbf{V}_1$ to $\mathbf{V}_4$ are the various compressor input voltages and are numbered according to Figure 4; $\mathbf{V}_1$ and $\mathbf{V}_2$ drive the coils of compressor 1; $\mathbf{V}_3$ and $\mathbf{V}_4$ drive those of compressor 2. The elements $\mathbf{H}_{ij}$ of matrix **H** are the transfer functions from voltage $\mathbf{V}_i$ to acceleration $\mathbf{A}_j$. In fact, equation (7) is frequency dependent; or in our case, it depends on which harmonic is considered. However, the subscript n denoting the various harmonics is omitted here. Also, it will be clear that the accelerations themselves are not available to the algorithm, but rather the outputs of the acceleration sensors. This is elaborated upon in section 4.

The matrix **H** is now simplified by making a few assumptions. Firstly, the input voltages influence only the compressor it drives and the displacer unit, which implies

$$\mathbf{H}_{12} = 0, \qquad \mathbf{H}_{22} = 0, \qquad \mathbf{H}_{31} = 0, \qquad \mathbf{H}_{41} = 0. \quad (8)$$

Secondly, due to symmetry in the cryocooler design, the following assumptions are also valid:

$$\mathbf{H}_{21} = -\mathbf{H}_{11}, \qquad \mathbf{H}_{42} = -\mathbf{H}_{32}, \quad (9)$$

$$\mathbf{H}_{23} = \mathbf{H}_{13}, \qquad \mathbf{H}_{43} = \mathbf{H}_{33}. \quad (10)$$

It is not allowed to relate directly $\mathbf{H}_{13}$ and $\mathbf{H}_{23}$ to $\mathbf{H}_{33}$ and $\mathbf{H}_{43}$ as the phase relation between the two compressors is not defined beforehand. By applying assumptions (8)–(10) to equation (7), the system can be described by

$$\begin{Bmatrix} \mathbf{A}_1 \\ \mathbf{A}_2 \\ \mathbf{A}_3 \end{Bmatrix}(k) = \begin{Bmatrix} \mathbf{D}_1 \\ \mathbf{D}_2 \\ \mathbf{D}_3 \end{Bmatrix} + \begin{bmatrix} \mathbf{H}_{11} & -\mathbf{H}_{11} & \mathbf{0} & \mathbf{0} \\ \mathbf{0} & \mathbf{0} & \mathbf{H}_{32} & -\mathbf{H}_{32} \\ \mathbf{H}_{13} & \mathbf{H}_{13} & \mathbf{H}_{33} & \mathbf{H}_{33} \end{bmatrix} \begin{Bmatrix} \mathbf{V}_1 \\ \mathbf{V}_2 \\ \mathbf{V}_3 \\ \mathbf{V}_4 \end{Bmatrix}(k). \quad (11)$$

Upon noting the symmetry in equation (11) it was decided not to use the input voltages as control voltages, but to introduce the control voltages $\mathbf{V}_{c1}$ to $\mathbf{V}_{c4}$ (see Figure 4): i.e.,

$$\begin{Bmatrix} \mathbf{A}_1 \\ \mathbf{A}_2 \\ \mathbf{A}_3 \end{Bmatrix}(k) = \begin{Bmatrix} \mathbf{D}_1 \\ \mathbf{D}_2 \\ \mathbf{D}_3 \end{Bmatrix} + \begin{bmatrix} \mathbf{G}_{11} & \mathbf{0} & \mathbf{0} & \mathbf{0} \\ \mathbf{0} & \mathbf{0} & \mathbf{G}_{32} & \mathbf{0} \\ \mathbf{0} & \mathbf{G}_{23} & \mathbf{0} & \mathbf{G}_{43} \end{bmatrix} \begin{Bmatrix} \mathbf{V}_{c1} \\ \mathbf{V}_{c2} \\ \mathbf{V}_{c3} \\ \mathbf{V}_{c4} \end{Bmatrix}(k). \quad (12)$$

The symbol $\mathbf{G}_{ij}$ is introduced for the various transfer functions from control voltage $\mathbf{V}_{ci}$ to acceleration $\mathbf{A}_j$. The requirement $\mathbf{A}_j(k+1) = \mathbf{0}$ leads to the control action defined by the equations

$$\mathbf{V}_{c1}(k+1) = \mathbf{V}_{c1}(k) - \mathbf{A}_1(k)/\mathbf{G}_{11}, \quad (13)$$

$$\mathbf{V}_{c2}(k+1) = \mathbf{V}_{c2}(k) - \alpha\mathbf{A}_3(k)/\mathbf{G}_{23}, \quad (14)$$

$$\mathbf{V}_{c3}(k+1) = \mathbf{V}_{c3}(k) - \mathbf{A}_2(k)/\mathbf{G}_{32}, \quad (15)$$

$$\mathbf{V}_{c4}(k+1) = \mathbf{V}_{c4}(k) - (1-\alpha)\mathbf{A}_3(k)/\mathbf{G}_{43}. \quad (16)$$

At this point, one is still free to choose phase and magnitude of the parameter α. This implies that the displacer vibration may be controlled with $\mathbf{V}_{c2}$ ($\alpha = 1$), $\mathbf{V}_{c4}$ ($\alpha = 0$), or some combination. In the next section we will add conditions to define the parameter α.

3.3. CONTROL RESTRICTIONS

To ease the load of a single cooler, it was decided to divide equally the control action over $\mathbf{V}_{c2}$ and $\mathbf{V}_{c4}$:

$$|\mathbf{V}_{c2,n}|^2 = |\mathbf{V}_{c4,n}|^2. \quad (17)$$

This equation states that the nth harmonic components in $\mathbf{V}_{c2}$ and $\mathbf{V}_{c4}$ are equal in size. Using the restriction equation (17) and the condition that both control voltages $\mathbf{V}_{c2}$ and $\mathbf{V}_{c4}$ have optimum phase for suppression of the acceleration (α is real), one finds

$$\alpha_n = \frac{|G_{23,n}|}{|G_{23,n}| + |G_{43,n}|}. \quad (18)$$

Thus, α is determined separately for each harmonic n. Combined with equations (14) and (16) the control action is now defined. However, due to the presence of the drive signal $\mathbf{V}_0$, equations (17) and (18) are inappropriate for the drive frequency. Theoretically, the system may reach a state without input voltage, as this obviously eliminates all vibrations. Therefore, a condition is used stating that the total power input of the cryocoolers should remain constant (second index 1 refers to the ground frequency):

$$|\mathbf{V}_{1,1}|^2 + |\mathbf{V}_{2,1}|^2 + |\mathbf{V}_{3,1}|^2 + |\mathbf{V}_{4,1}|^2 = 4|\mathbf{V}_0|^2. \quad (19)$$

This equation states that the total power input is independent of the control voltages. Upon neglecting the control voltages $\mathbf{V}_{c1}$ and $\mathbf{V}_{c3}$, this is equivalent to

$$|\mathbf{V}^*_{1,1}|^2 + |\mathbf{V}^*_{2,1}|^2 = |\mathbf{V}_0 + \mathbf{V}_{c2,1}|^2 + |\mathbf{V}_0 + \mathbf{V}_{c4,1}|^2 = 2|\mathbf{V}_0|^2. \tag{20}$$

To satisfy condition (20), the drive frequency components of $\mathbf{V}_{c2}$ and $\mathbf{V}_{c4}$ are calculated by using the following three steps

1. The drive frequency components of the control voltages $\mathbf{V}_{c2}$ and $\mathbf{V}_{c4}$ are updated with equations (14) and (16) using $\alpha_1 = 1$.

2. The resulting $\mathbf{V}^*_{1,1}$ and $\mathbf{V}^*_{2,1}$ are scaled with a complex parameter κ. The amplitude of the parameter is determined by the restriction of constant power. For reasons of symmetry, the phase of κ is chosen such that $\mathbf{V}^*_{1,1}$ and $\mathbf{V}^*_{2,1}$ are placed symmetrically around the original drive voltage $\mathbf{V}_0$. In order to facilitate calculations, the parameter κ was calculated to satisfy

$$|\mathbf{V}^*_{1,1}| + |\mathbf{V}^*_{2,1}| = 2|\mathbf{V}_0|, \tag{21}$$

which is a linear approximation of equation (20).

3. $\mathbf{V}_{c2,1}$ and $\mathbf{V}_{c4,1}$ are calculated by subtracting $\mathbf{V}_0$ from $\mathbf{V}^*_{1,1}$ and $\mathbf{V}^*_{2,1}$.

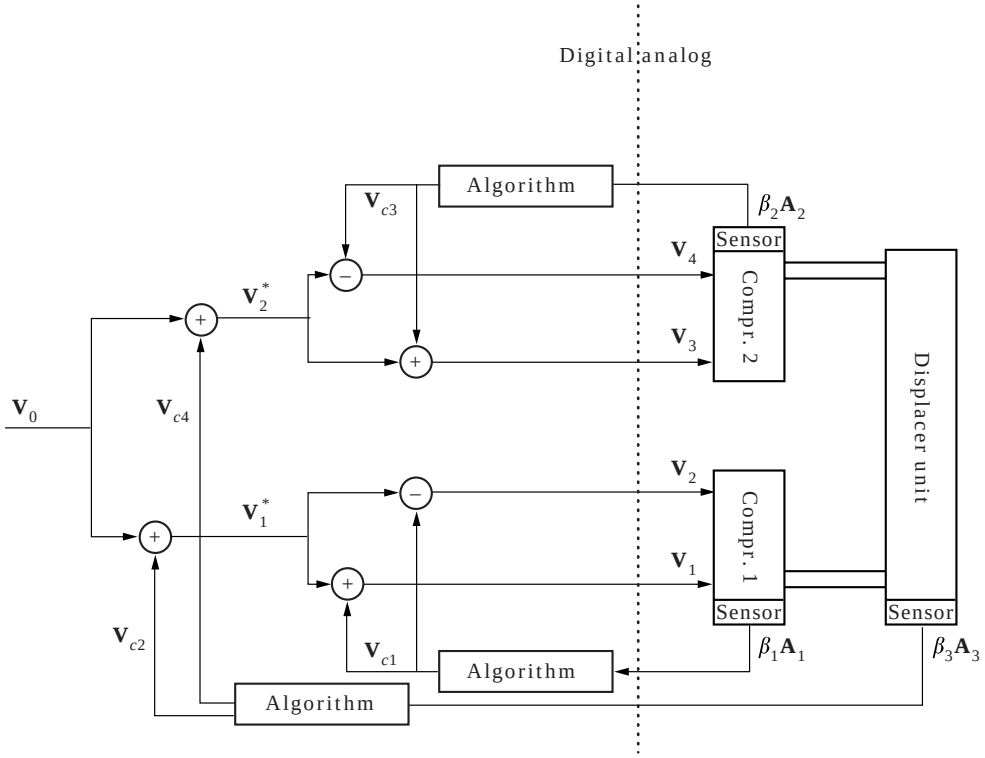

Figure 4. Schematic representation of the control system. The drive voltage $\mathbf{V}_0$, the control voltages $\mathbf{V}_{c1}$ and $\mathbf{V}_{c3}$ to control the compressors, and $\mathbf{V}_{c2}$ and $\mathbf{V}_{c4}$ for controlling the vibrations of the displacer unit are shown.

4. TRANSFER FUNCTIONS

Before applying a control action, the transfer functions $\mathbf{G}_{ij}$ are determined in a three-step procedure, as follows.

1. Measurement of the vibration $\mathbf{A}_j(k)$.
2. Change of $\mathbf{V}_{ci}(k)$ with a known amount $\Delta\mathbf{V}_{ci}$.
3. Measurement of $\mathbf{A}_j(k+1)$ and calculation of the transfer function $\mathbf{G}_{ij}$ by use of equation (22). This equation is derived by using equation (2), upon assuming the transfer function $\mathbf{G}_{ij}$—i.e., $\mathbf{H}$ in equation (2)—to be the only unknown:

$$\mathbf{G}_{ij} = 2\,\frac{\mathbf{A}_j(k+1) - \mathbf{A}_j(k)}{\Delta\mathbf{V}_{ci}}\,. \tag{22}$$

This procedure is repeated for each relevant harmonic and each transfer function. In principle all harmonics of the transfer functions could be simultaneously measured, but to prevent inaccuracies due to cross-over, they were measured separately.

Both the acceleration sampling and the DFT calculation consume time, which puts a limit on the response time of the control system. Having calculated $\mathbf{V}(k)$ for one complete period and having stored the data for continuous read-out, it is clear that $\mathbf{V}(k+1)$ cannot be calculated from $\mathbf{A}(k)$ as expressed in equation (3). The storage takes *ca*. 0·5 s. The transient responses are then given another 25 drive frequency periods to die out. $\mathbf{A}(k)$ is determined by calculating the DFT for the next 25 periods. Thus, the period for the control action (*ca*. 1·5 s) is approximately 75 times the period of the 1 drive frequency.

In fact, not the acceleration $\mathbf{A}$ is measured, but the sensor response to $\mathbf{A}$: $\beta\mathbf{A}$. Therefore, $\beta\mathbf{G}$ is determined and not $\mathbf{G}$. This is not a problem as e.g., equations (13) and (22) have the following equivalents:

$$\mathbf{V}_{c1}(k+1) = \mathbf{V}_{c1}(k) - \frac{(\beta\mathbf{A})_1(k)}{(\beta\mathbf{G})_{11}}\,, \qquad (\beta\mathbf{G})_{11} = \frac{(\beta\mathbf{A})_1(k+1) - (\beta\mathbf{A})_1(k)}{\Delta\mathbf{V}_{c1}}\,. \tag{23, 24}$$

This means the sensor output is controlled and not the acceleration. However, if the sensor is fast as compared to the process and has a significant response in the frequency range of interest, the acceleration is also controlled. In the sensor function β we also include any sampling delays. Furthermore, it should be noted that the control voltages are digital variables. Therefore, the behaviour of the AD-converters and amplifiers is also included in the transfer functions.

In order to ensure convergence of the control system, the error in determining the transfer function should be such that an acceleration caused by a random disturbance does not increase in successive control steps. The following equation is derived from equations (1)–(3) and gives the acceleration $\mathbf{A}(k+1)$ resulting from the measured acceleration $\mathbf{A}(k)$:

$$\mathbf{A}(k+1) = \left(1 - \frac{\mathbf{G}}{\tilde{\mathbf{G}}}\right)\mathbf{A}(k). \tag{25}$$

In this equation $\tilde{\mathbf{G}}$ represents the measured transfer function, i.e., the exact transfer function plus the error upon measurement. This means, for proper control, the following inequality is required:

$$|1 - \mathbf{G}/\tilde{\mathbf{G}}| < 1. \tag{26}$$

If $\mathbf{G} = \tilde{\mathbf{G}}$ for all harmonics, there is in principle one-step reduction of the vibrations. Also equation (26) shows that by choosing $\tilde{\mathbf{G}}$ too large, the probability of a stable control algorithm is improved although it does slow the process of vibration reduction.

5. HARDWARE

Figure 5 is a schematic representation of the experimental set-up. It contains the two cryocoolers with the cold heads combined to a single unit. The base plate as mentioned in section 2 and described elsewhere [6] is used. The positioning of the compressors and the displacer unit corresponds to Figure 2. The compressor vibrations are measured using acceleration transducers of the type Seika BDK3 (accuracy 0·02 ms^{-2}; sensitivity 0·013 V/ms^{-2} and range 30 ms^{-2}). For measurement of the displacer unit's acceleration a Bruël & Kjær (B&K) 4381 sensor with pre-amplifier was available (accuracy and sensitivity 0·002 ms^{-2} and 0·32 V/ms^{-2}, respectively).

The sensor outputs are filtered by fourth-order Butterworth filters with cut-off frequencies of 500 Hz. The filtered signals are sampled by a DAP-board type 2400/e4 from Microstar Laboratories. For the BDK3 and B&K an on-board gain of respectively 100 and 10 is used followed by a 12-bit DA-converter at 1024 Hz. Having completed a Discrete Fourier Transform the DAP-board sends the data to the PC. The PC determines the new values for the control variables and calculates the coil voltages for a full period. In the next step the calculated voltages are copied to the so-called ringbuffer.

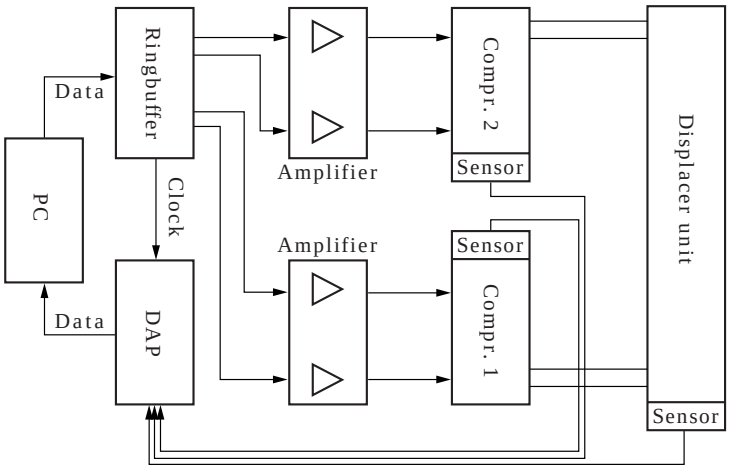

Figure 5. Schematic diagram of the experimental set-up.

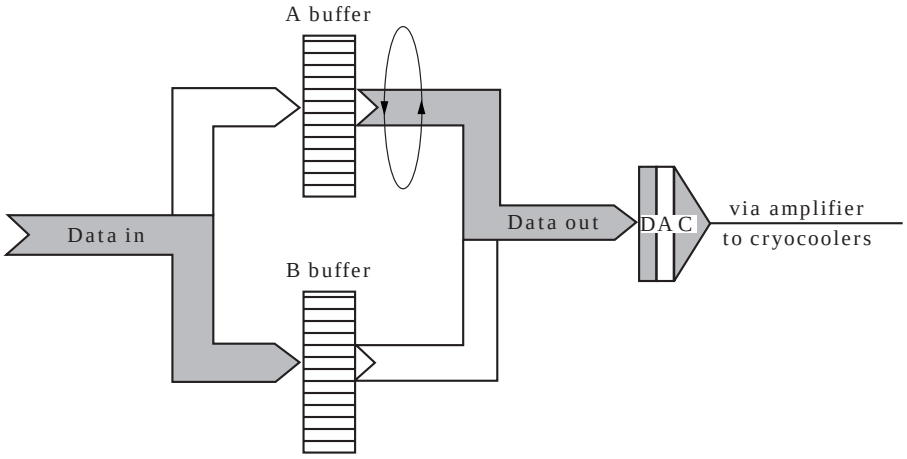

Figure 6. Diagram of the ringbuffer design.

This ringbuffer is an especially designed interface between the PC and two commercial audio amplifiers. It consists of two sets of four buffers, four DA-converters (DAC) and some logic. Whilst one set of buffers is circularly read to provide the coil voltages, the other may be defined by computer (see Figure 6). When the new coil voltages are written, the computer can order the ringbuffer to switch sets and use the new data to define the coil voltages. The other set of buffers is then available for updating. Another feature of the ringbuffer is the clock-signal. The clock used by the DAP-board for sampling, is defined by the ringbuffer. This ensures a lasting synchronization between the coil voltages and sampling. If this synchronization does not exist the measured phase of the transfer functions is meaningless and the control system will fail.

The functional lay-out of the ringbuffer is depicted in Figure 7. The controller is formed by an FPGA (Field Programmable Gate Array). A crystal oscillator circuit supplies a 19·6608 MHz clock signal for internal synchronization of the FPGA-operations. It is also the source from which the FPGA derives both the 1024 Hz sampling clock and the 50 Hz for the cooler frequency. The cryocooler input signal is defined by 8192 points. Therefore, the four DACs are each updated from the on-board memory with a frequency of $8192 * 50$ Hz. The SRAM type memory facilitates calibration of the coolers drive voltages by computer and subsequent use of this data without computer back-up. To this end, the board is also provided with its own power supply.

The PC connection is realised through the parallel port. Data and commands are placed on the data lines. The control and status lines are used for the communication protocol. To ensure that the sampling clock start is synchronized with the DAC-signals, commands are executed once every 20 ms. This moment is determined by testing the address register used for continuously sending data from the buffer memory to the DACs. Commands are executed when the address equals zero.

6. EXPERIMENTAL RESULTS

During the first 50 min of operation, drift was observed in the transfer functions. This is probably due to changes in mechanical properties caused by cooling down of the cold head and warming up of the compressors. Therefore, all measurements were performed after a period of about 50 min.

The assumptions made in section 3 necessary for correct operation of the basic algorithm are linearity of the system and presence of only a restricted number of harmonics. Figures 8 and 9 show that the assumption of linearity is adequate to ensure convergence. Figure 8 shows the change of the harmonic components in the acceleration of a compressor when a certain frequency component is added to one of the coil voltages. The figure shows clearly that a frequency component added to a coil voltage leads primarily to additional compressor vibrations with the same frequency. To be more quantitative, factor C is introduced as a measure for the crosstalk between two frequencies. For the combination of 50 and 100 Hz, this factor is

$$C_{50,100} = \sqrt{M_{50,100} * M_{100,50}/M_{50,50} * M_{100,100}} \approx 0{\cdot}07.$$

Here, M denotes the 10×10 matrix shown in the figure, whereas the subscripts denote the frequencies in question. Analogously, for 450 and 500 Hz, the factor is

$$C_{450,500} = \sqrt{M_{450,500} * M_{500,450}/M_{450,450} * M_{500,500}} \approx 0{\cdot}04.$$

These, and also the other crosstalk factors are well below one, and therefore, the error made by assuming the system to be linear is quite small. Figure 9 shows the same graph for the transfer function from the control voltage V_{c2} to the acceleration of the displacer unit. As the transfer from input voltage to displacer vibration is clearly less direct than the relation between voltage and compressor

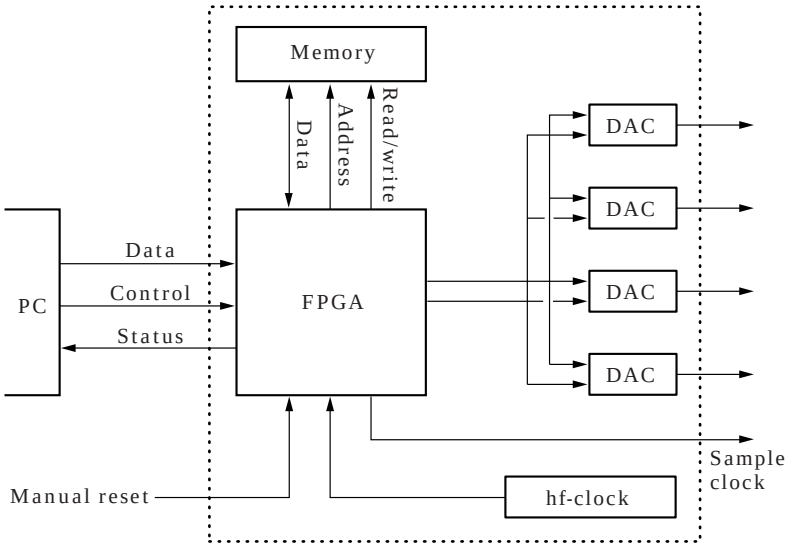

Figure 7. Representation of the functional lay-out of the ringbuffer.

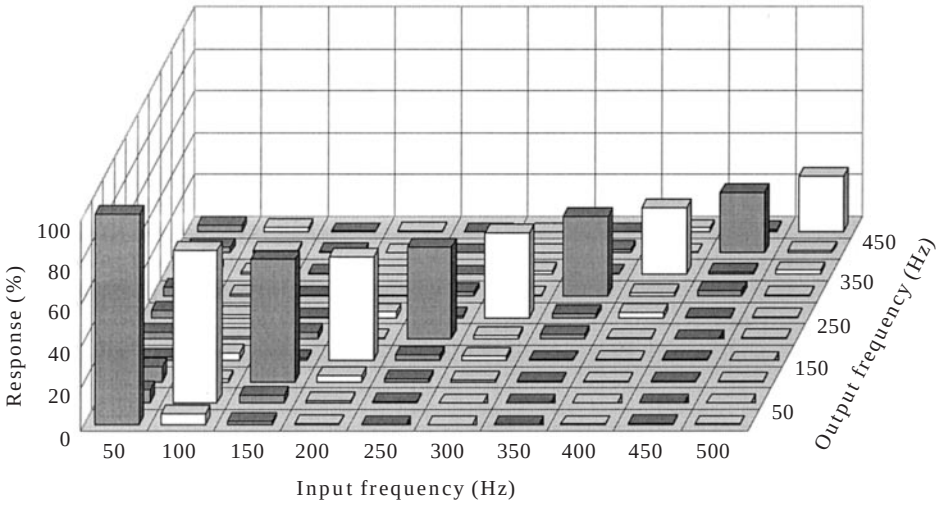

Figure 8. Response of the compressor acceleration to a change in the compressor coil voltage at a specific frequency. The largest value is scaled to unity. The others are scaled accordingly.

vibration, the non-linearity in this case is larger: $C_{50,100} \approx 0{\cdot}2$; $C_{450,500} \approx 0{\cdot}6$. This non-linearity will decrease the convergence in a way equivalent to a time-varying disturbance. The description of the initial disturbance with harmonics is also accurate, as can be seen in Figures 10 and 11. Figure 10 shows the initial and controlled vibrations of a compressor unit in logarithmic scale. Figure 11 shows the same for the displacer unit.

Assumptions made in section 3.2 concern the mutual relations of the transfer functions, such as opposing transfer functions for both coils of one cooler to the compressor vibration. These assumptions were verified and found to be valid, although the assumption that both inputs of one compressor have equal effect on

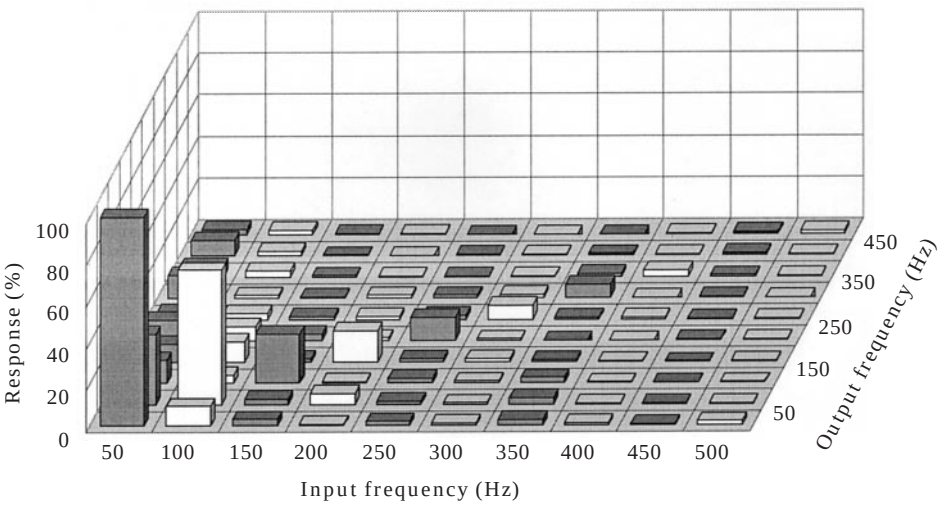

Figure 9. Response of the displacer unit acceleration to a change in the control voltage $\mathbf{V}_{c2}$ at a specific frequency. The largest value is scaled to unity. The others are scaled accordingly.

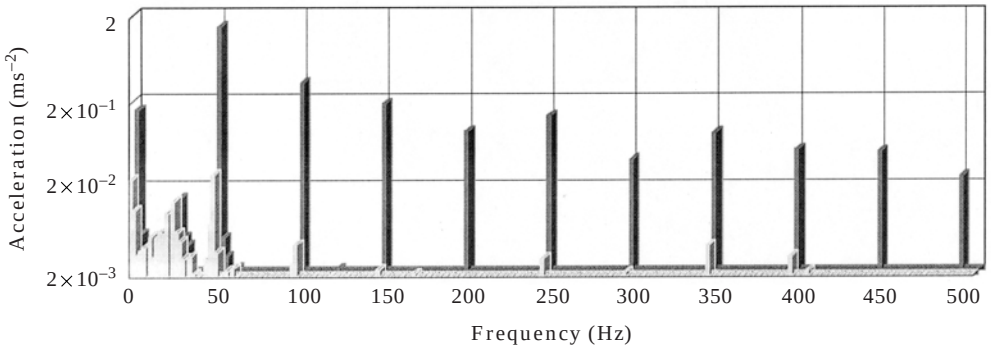

Figure 10. Acceleration of a compressor on a logarithmic scale. The graph in the back shows the vibration without control. The graph in front shows the remaining vibration when the control system is used.

the displacer unit (equation (10)), appeared to hold only for the harmonics up to about 200 Hz. This is probably caused by the mechanical coupling between the compressor and the cold head taking over the effect of the coupling by gas pressure.

The convergence of the control system is excellent. This is seen in Figure 12 for the 50 Hz components of the acceleration. For higher harmonics similar graphs were obtained. As the algorithm is a one-step control algorithm, the acceleration may be reduced to the vibration sensors' noise level in a single control step. However, to protect the amplifiers and coolers from transient phenomena, only limited changes in coil voltages were allowed during each control step. For this reason multiple steps are applied in practice, as is visible in Figure 12.

Figures 10 and 11 show vibrations of a compressor and the displacer unit with and without use of the control system. For clarity, aliasing peaks present in the original recordings are omitted. Because they do not interfere with the peaks shown, they are easy to eliminate. Averaging over about 20 measurements gives the following results. The compressor vibrations are reduced by a factor 50 from 1 to 0·02 ms^{-2}. The displacer unit's acceleration is reduced from 0·2 to 0·01 ms^{-2}.

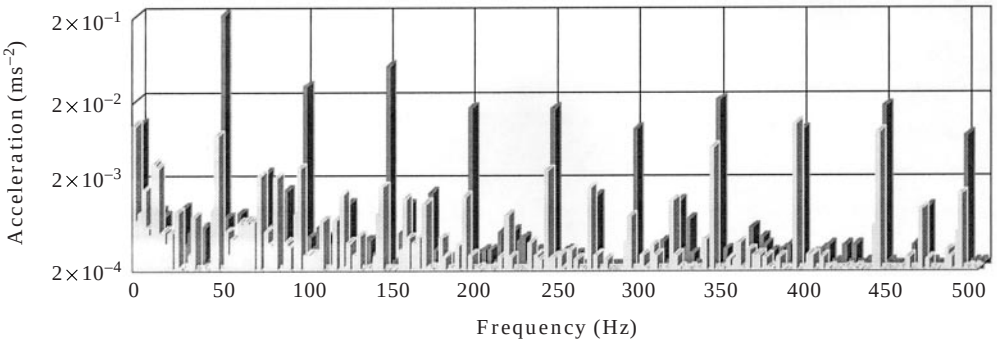

Figure 11. Acceleration of the displacer unit on a logarithmic scale. The graph in the back shows the vibration without control. The graph in front shows the remaining vibration when the control system is used.

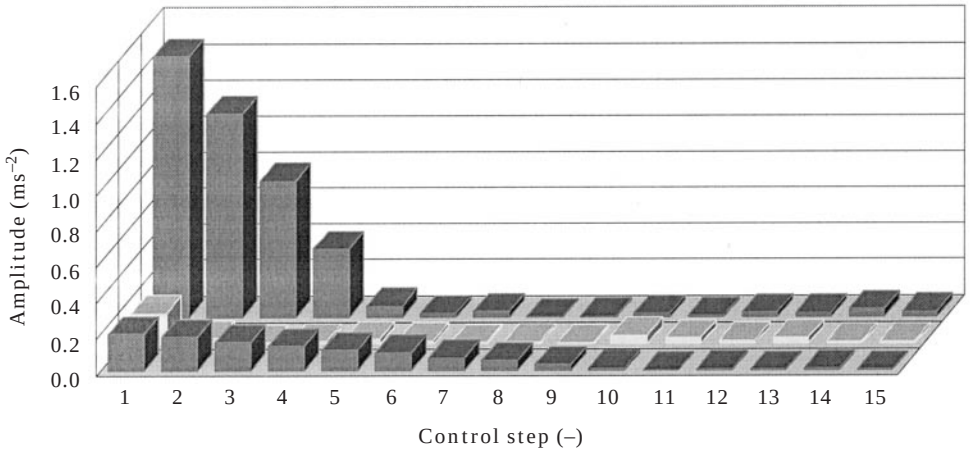

Figure 12. Acceleration sequence measured for the first 15 control steps. From back to front the acceleration is shown for compressor 1, compressor 2 and the displacer unit.

It is expected that use of more accurate acceleration transducers may reduce the vibrations of the compressors by an additional factor of five. It is anticipated that the reduction of displacer unit vibration is limited by discrepancies in the synchronization between sampling and drive voltage. One measurement, carried out with an *ad hoc* solution to prevent these discrepancies, resulted in a vibration level for the displacer unit of only 0·002 ms^{-2}. This corresponds to the noise level of the unit acceleration sensor. This discrepancy should not occur in the outlined control system, but is probably due to compatibility problems in the sample clock connection from ringbuffer to DAP-board.

7. CONCLUDING REMARKS

Based on the algorithm described by Wu [7], a control system was developed, capable of simultaneously reducing the vibration for all three components: i.e., the two compressors and the displacer unit. In principle, all vibrations can be reduced to the intrinsic noise level in just one control step, although inaccuracies in the measured transfer functions will limit the convergence. By using this control system the vibration levels in the axial direction are reduced from 1 to 0·02 ms^{-2} for the compressor modules and from 0·2 to 0·01 ms^{-2} for the displacer unit. The vibrations that remain are smaller than those which were measured perpendicular to that axis. These are found to have a magnitude of 0·05 ms^{-2}.

ACKNOWLEDGMENTS

The authors would like to thank the co-workers of Signaal USFA for their contribution in the discussions. Further, we are indebted to the Electronics Advice and Standardisation group of the Department of Applied Physics for their work on realizing the ringbuffer, to H. te Veene for his technical support during the experimental phase and to M. Smithers for his comments on the text of the manuscript.

REFERENCES

1. J. Clarke 1994 *Scientific American* **271**, 36–43. SQUIDS.
2. P. J. van den Bosch, H. J. M. ter Brake, H. J. Holland, H. A. de Boer, J. F. C. Verberne and H. Rogalla 1997 *Cryogenics* **37**, 139–151. Cryogenic design of a high-Tc SQUID-based heart scanner cooled by small Stirling cryocoolers.
3. H. J. M. ter Brake, P. J. van den Bosch, W. A. M. Aarnink, H. J. Holland, J. Flokstra and H. Rogalla 1995 *Applied Superconductivity* 1995, *Edinburgh*, 1503–1506. Design aspects of a high-Tc SQUID based heart scanner.
4. D. Verbeek, H. Helmonds and P. Roos 1992 *Proceedings of the 7th International Cryocooler Conference*, *Santa Fe*, 728–737. Performance of the Signaal USFA Stirling cooling engines.
5. G. Walker 1989 *Miniature Refrigerators for Cryogenic Sensors and Cold Electronics*. Oxford: Clarendon Press.
6. J. F. C. Verberne, P. C. Bruins, P. J. van den Bosch and H. J. M. ter Brake 1995 in *Cryocooler* 8; 465–474. New York: Plenum Press. Reduction of the vibrations generated by Stirling cryocoolers for cooling a high Tc SQUID magnetometer.
7. Y. A. Wu 1994 *Advances in Cryogenic Engineering* **39**(B), 1271–1280. New York: Plenum Press. Active vibration control algorithm for cryocooler.
8. R. Boyle, F. Conners, J. Marketon, V. Arillo, E. James and R. Fink 1992 *Proceedings of the 7th International Cryocooler Conference*, *Santa Fe*, 805–819. Non-real time feed forward vibration control system development & test results.